Generation of *n*-Dimensional Hyperchaotic Maps Using Gershgorin-Type Theorem and Its Application

Yinxing Zhang, Zhongyun Hua, *Senior Member, IEEE*, Han Bao, *Member, IEEE*, Hejiao Huang, and Yicong Zhou, *Senior Member, IEEE*

***Abstract*—High-dimensional (HD) chaotic map has wide applications in various research fields such as neural networks and secure communication. Designing HD chaotic maps with expected dynamics and robust hyperchaotic behaviors is an interesting but challenging topic. In this article, we propose an *n*-dimensional hyperchaotic map (*n*D-HCM) generation method on the basis of the Gershgorin-type theorem. First, the general form of the proposed *n*D-HCM is built using *n* parametric polynomials. Then, the entity and coefficient parameter matrices are configured according to the Gershorin-type theorem. Theoretical analysis shows that the generated *n*D-HCM has *n* positive Lyapunov exponents and thus can show robust hyperchaotic behaviors. Two examples of hyperchaotic map with specified equations are provided and their properties are analyzed to show the availability of the proposed method. Performance evaluations display that our *n*D-HCM possesses abundant properties and complex behaviors, and it can outperform some representative HD chaotic maps. Moreover, to show the application of our *n*D-HCM, we apply it to a secure communication scheme and the experimental results exhibit that it shows much better performance than these representative HD chaotic maps in resisting transmission noise.**

***Index Terms*—Chaos, hyperchaos, hyperchaotic behavior, nonlinear system, secure communication.**

Manuscript received 27 December 2022; accepted 29 May 2023. Date of publication 23 June 2023; date of current version 18 September 2023. This work was supported in part by the National Natural Science Foundation of China under Grant 62071142 and Grant 62201094; in part by the Guangdong Basic and Applied Basic Research Foundation under Grant 2021A1515011406; in part by the Shenzhen College Stability Support Plan under Grant GXWD20201230155427003-20200824210638001; and in part by the Guangdong Provincial Key Laboratory of Novel Security Intelligence Technologies under Grant 2022B1212010005. This article was recommended by Associate Editor S. Xie. *(Corresponding author: Zhongyun Hua.)*

Yinxing Zhang is with the School of Computer Science and Technology, Harbin Institute of Technology, Shenzhen, Shenzhen 518055, China (e-mail: yxzhang23@163.com).

Zhongyun Hua and Hejiao Huang are with the School of Computer Science and Technology, Harbin Institute of Technology, Shenzhen, Shenzhen 518055, China, and also with the Guangdong Provincial Key Laboratory of Novel Security Intelligence Technologies, Shenzhen 518055, China (e-mail: huazyum@gmail.com; huanghejiao@hit.edu.cn).

Han Bao is with the School of Microelectronics and Control Engineering, Changzhou University, Changzhou 213164, China (e-mail: charlesbao0319@gmail.com).

Yicong Zhou is with the Department of Computer and Information Science, University of Macau, Macau, China (e-mail: yicongzhou@umac.mo).

Color versions of one or more figures in this article are available at https://doi.org/10.1109/TSMC.2023.3283433.

Digital Object Identifier 10.1109/TSMC.2023.3283433

I. Introduction

NONLINEAR system is a wide research subject [1], [2] and it plays a very important role in various research fields [3], [4], for example, artificial intelligence [5]. Chaotic signal is a kind of nonlinear signals and it was first observed in meteorology [6]. Since the 21st century, the chaotic signal attracts increasing attentions from the researchers of artificial intelligence [7], [8]. A chaotic system is a kind of nonlinear systems with initial state dependence, and it possesses many unique characteristics such as initial value sensitivity, randomness, ergodicity, and unpredictability [9]. With these properties, chaotic systems can be extensively applied in almost all the research and engineering fields [10], [11], [12], such as image encryption [13], [14] and secure communication [15], [16].

According to the number of dimensions, all the chaotic maps are classified into two categories: 1) low-dimensional (LD) chaotic map and 2) high-dimensional (HD) chaotic map [9], [17]. The LD chaotic maps have simple structures and require small implementation cost. However, researchers found that existing LD chaotic maps may have many property limitations. First, the chaotic ranges of many LD chaotic maps are discontinuous and this leads to weak ability to resist chaos degradation [18]. The chaos degradation indicates that the chaos properties of a chaotic map disappear in digit domain because of the finite precision. With weak ability of resisting chaos degradation, the LD chaotic maps have serious security problems when being applied to many applications [19]. Besides, many existing LD chaotic maps cannot show hyperchaotic behaviors. The hyperchaotic behavior is a kind of more complex behavior than the chaotic behavior, and a globally bounded chaotic system with more than one positive Lyapunov exponent (LE) exhibits hyperchaotic behavior.

To overcome the performance limitations of existing LD chaotic maps, researchers improve the performance of existing LD chaotic maps by perturbing the variables or parameters [20], or directly construct new LD chaotic maps with better performance [21], [22]. These works can well address the problems of the LD chaotic maps in lacking discontinuous chaotic intervals and hyperchaotic behaviors [21], [22]. However, since an LD chaotic map has a small dimension space, its behaviors are easier to be predicted using some artificial intelligence techniques [23], [24] than the HD

chaotic maps. If the signals of a chaotic map are accurately predicted, the chaotic map will lose its unpredictability, and this leads to the failures of the practical applications using it [25]. Besides, the chaos properties of many new LD chaotic maps lack theoretical guarantees [21], [22].

Compared with the LD chaotic maps, the HD chaotic maps require more implementation cost and are more difficult to be implemented in some hardware platforms. However, they have large dimension space and their behaviors are unpredictable. Besides, they usually have more parameters and variables and thus show more complex behaviors than the LD chaotic maps [26]. Up to now, researchers have constructed many HD chaotic systems/maps [27], [28], [29]. For example, Lassoued and Boubaker [30] proposed nine four-dimensional chaotic systems that have two positive LEs by introducing a controller to existing three-dimensional (3-D) chaotic systems. This method can only construct HD chaotic systems with two positive LEs, and cannot construct chaotic systems with more positive LEs. According to the discussions in [31], the complexity of an HD chaotic system/map is highly dependent of its number of positive LEs. A chaotic system/map with very high dimension cannot show complex behavior if it only has a small number of positive LEs. Thus, the main purpose of designing HD chaotic systems/maps is to obtain more positive LEs while keeping the dimension as low as possible.

To design HD hyperchaotic systems/maps with a large number of positive LEs, researchers have developed many methods using different techniques [32], [33]. For example, Shen et al. [33] developed an nD continuous chaotic system generation method, which can generate chaotic systems with $\lfloor n-1 \rfloor/2$ positive LEs. Wu et al. [34] proposed a Laplace expansion method that can produce HD Cat maps with multiple positive LEs and thus show complex behaviors. These generation methods are able to construct HD hyperchaotic systems/maps with multiple and even maximum number of positive LEs, which result in quite complex hyperchaotic behaviors [11], [31]. However, the effects of these methods highly rely on the designer's experience in debugging parameters. When constructing hyperchaotic systems/maps with desired property, one should try many potential parameter values to determine the proper ones, which lacks of robustness. Besides, the outputs of these hyperchaotic systems/maps can only distribute on a small area of the phase space. Thus, designing HD hyperchaotic systems/maps with expected dynamics and robust hyperchaotic behaviors is a meaningful but challenging topic.

To generate HD hyperchaotic maps (HCMs) with expected dynamics and robust hyperchaotic behaviors, we propose an n-dimensional HCM (nD-HCM) generation method. First, we construct the general form of the proposed nD-HCM from n parametric polynomials with arbitrary order. Then, we configure the entity parameter matrix and coefficient parameter matrix on the basis of the Gershgorin-type theorem. Using different settings of the entity parameter matrix and coefficient parameter matrix, a large number of new nD-HCMs can be generated. Theoretical analysis indicates that the produced nD-HCMs possess n positive LEs and thus can show robust hyperchaotic behaviors. To exhibit the effect of the proposed method, we generate two HCMs as examples including a three-dimensional HCM (3D-HCM) and a nine-dimensional HCM (9D-HCM). Property analysis shows the robust hyperchaotic behaviors of the 3D-HCM and 9D-HCM. Performance evaluations and comparisons show that the generated nD-HCMs have complex and robust hyperchaotic behaviors, and show much better performance than some representative HD chaotic maps. To further show the application of our nD-HCM, we apply the nD-HCMs generated by our method to the application of secure communication. Test results demonstrate that they show better performance than the representative HD chaotic maps in resisting channel noise.

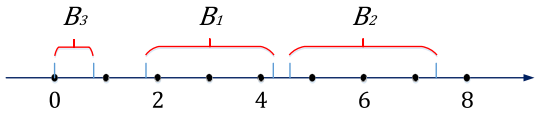

Fig. 1. Demonstrations of the three real intervals in the 3×3 square matrix shown in (1).

The remainder of this article is organized as follows. Section II presents the Gershgorin-type theorem as a background. Section III introduces the proposed nD-HCM generation method and theoretically analyzes its hyperchaotic behaviors. Section IV provides two examples of nD-HCM and analyzes their properties. Section V tests the performance of the proposed nD-HCM. Section VI explores the effect of our nD-HCM on secure communication. Section VII concludes this article.

II. Gershgorin-Type Theorem

This section introduces the Gershgorin-type theorem [35], [36] and deduces a lemma using the theorem to explore the properties of matrix.

A. Gershgorin-Type Theorem

First, we define the real interval in Definition 1 and review the Gershgorin-type theorem in Theorem 1.

Definition 1: Let $A = (a_{kj})^{n\times n}$ be a complex square matrix, and $R_k = \sum_{\substack{j=1 \\ j\neq k}}^{n} |a_{kj}|$ and $C_k = \sum_{\substack{j=1 \\ j\neq k}}^{n} |a_{jk}|$ be the sums of the absolute values of the nondiagonal elements in the kth row and column of A, respectively. A real interval B_k centered at a_{kk} is defined as $B_k = [(|a_{kk}| - s_k)_+, |a_{kk}| + s_k]$, where s_k is the radius and $s_k = \max\{R_k, C_k\}$, and $a_+ = \max\{0, a\}$.

Suppose a square matrix A with size 3×3 is defined as

$$A = \begin{pmatrix} 3 & 0.2 & -0.2 \\ 1 & -6 & 0.4 \\ 0.2 & 0.5 & -0.1 \end{pmatrix}. \tag{1}$$

Its three real intervals can be obtained as

$$B_1 = \left[(3-(1+0.2))_+, 3+(1+0.2)\right] = [1.8, 4.2]$$
$$B_2 = \left[(6-(1+0.4))_+, 6+(1+0.4)\right] = [4.6, 7.4]$$
$$B_3 = \left[(0.1-(0.2+0.5))_+, 0.1+(0.2+0.5)\right] = [0, 0.8]$$

and their representations in the real axis can be shown in Fig. 1. By defining the real intervals, one can estimate the

singular values of a square matrix by the Gershgorin-type theorem which is defined in Theorem 1.

Theorem 1 [35]: The n singular values of an $n \times n$ square matrix A are all within the corresponding real intervals of A.

For example, the three singular values of matrix A in (1) are $\sigma_1 = 3.0210$, $\sigma_2 = 7.2948$, and $\sigma_3 = 0.1978$, which all locate into their related real intervals.

From the Gerschgorin-type theorem, it is obvious that the n singular values of an $n \times n$ square matrix are within its related n real intervals. Using this principle, the lower bound of the n singular values of an $n \times n$ square matrix can be determined by presetting the real intervals using the matrix elements.

B. Properties of Matrix

According to the Gershgorin-type theorem presented in Theorem 1, we can deduce Lemma 1 that describes the lower bound of the n singular values in an $n \times n$ square matrix.

Lemma 1: Let $0 \le \sigma_1 \le \sigma_2 \le \cdots \le \sigma_n$ be the n singular values of the square matrix $A = (a_{ij})_{n\times n}$ and δ is an arbitrary positive constant. There exists

$$\sigma_k > \delta \tag{2}$$

if A satisfies that

$$|a_{kk}| > s_k + \delta \tag{3}$$

where $s_k = \max\{R_k, C_k\}$ denotes the radius of the ith real interval, $R_k = \sum_{\substack{j=1 \\ j\neq k}}^{n} |a_{kj}|$ and $C_k = \sum_{\substack{j=1 \\ j\neq k}}^{n} |a_{jk}|$.

Proof: Because the principal diagonal elements of the square matrix A satisfy $|a_{kk}| > s_k + \delta$, one can get

$$|a_{kk}| - s_k > \delta > 0. \tag{4}$$

From Definition 1, the n real intervals of A are

$$B_k = \left[(|a_{kk}| - s_k)_+, |a_{kk}| + s_k\right]$$

where $k = 1, 2, \ldots, n$. Let $\zeta = \min\{(|a_{11}| - s_1)_+, (|a_{22}| - s_2)_+, \ldots, (|a_{nn}| - s_n)_+\}$ be the lower bound of the real intervals B_k. From (4), one can obtain

$$\zeta > \delta > 0. \tag{5}$$

According to the Gershgorin-type theorem in Theorem 1, for $k = 1, 2, \ldots, n$, we can obtain that the each singular value of A satisfies

$$\sigma_k \ge \zeta. \tag{6}$$

Combining inequalities (5) and (6), we can get $\sigma_k > \delta$. So does the proof. ∎

Lemma 1 displays that all singular values of an nD matrix can be greater than any given positive values when some conditions between its main diagonal and nondiagonal elements are satisfied. For an nD matrix, its eigenvalues are related to its singular values. Moreover, the chaotic behaviors of a nonlinear system can be indicated by its LEs that is related to the eigenvalues of its parameter matrix. Therefore, using Lemma 1, one can configure the parameter matrix of an nD chaotic map, ensuring that the chaotic map shows robust hyperchaotic behaviors.

III. n-Dimensional Hyperchaotic Map Generation Method

This section first presents the general form of our nD-HCM, and then introduces a methodology to configure its parameter matrices. Finally, this section studies the hyerchaotic behaviors of the proposed nD-HCM.

A. General Form of the Proposed nD-HCM

The nD-HCM is built using n parametric polynomials. First, initialize n parametric polynomials with any order, and the general form is described as

$$x(i+1) = G(x(i)) \mod N \tag{7}$$

where $x(i) = \{x_1(i), x_2(i), \ldots, x_n(i)\}^T \in \mathbb{R}^{n\times 1}$ is the state vector at observation time i, N is an integer that acts as the modular coefficient, $G(x) : I^n \to I^n$ is a vector function and its detailed equations are expressed as

$$\begin{cases} x_1(i+1) = a_{11}x_1(i) + a_{12}x_2(i)^{c_{12}} + \cdots + a_{1n}x_n(i)^{c_{1n}} \\ x_2(i+1) = a_{21}x_1(i)^{c_{21}} + a_{22}x_2(i) + \cdots + a_{2n}x_n(i)^{c_{2n}} \\ \qquad\qquad \vdots \\ x_n(i+1) = a_{n1}x_1(i)^{c_{n1}} + a_{n2}x_2(i)^{c_{n2}} + \cdots + a_{nn}x_n(i). \end{cases} \tag{8}$$

It is obvious that all the control parameters in the nD-HCM can be classified into two categories: 1) entity parameters and 2) coefficient parameters. The entity parameters are to linearly change the iteration states while the coefficient parameters change the iteration states in nonlinear ways. All the entity parameters and coefficient parameters in the nD-HCM can be represented as

$$A = \begin{pmatrix} a_{11} & a_{12} & \cdots & a_{1n} \\ a_{21} & a_{22} & \cdots & a_{2n} \\ \vdots & \vdots & \ddots & \vdots \\ a_{n1} & a_{n2} & \cdots & a_{nn} \end{pmatrix} \tag{9}$$

and

$$C = \begin{pmatrix} 1 & c_{12} & \cdots & c_{1n} \\ c_{21} & 1 & \cdots & c_{2n} \\ \vdots & \vdots & \ddots & \vdots \\ c_{n1} & c_{n2} & \cdots & 1 \end{pmatrix} \tag{10}$$

respectively. Thus, the properties of the nD-HCM are determined by its entity parameter matrix A and coefficient parameter matrix C. By setting A and C as proper values, the nD-HCM can achieve hyperchaotic behaviors and desired dynamics.

B. Methodology of Configuring A and C

The Jacobian matrix $J(x(i))$ of the general form of the nD-HCM with respect to the observation state $x(i) = \{x_1(i), x_2(i), \ldots, x_n(i)\}^T \in \mathbb{R}^{n\times 1}$ can be described as follows:

$$J(x(i)) = \begin{pmatrix} a_{11} & a_{12}c_{12}x_2(i)^{c_{12}-1} & \cdots & a_{1n}c_{1n}x_n(i)^{c_{1n}-1} \\ a_{21}c_{21}x_1(i)^{c_{21}-1} & a_{22} & \cdots & a_{2n}c_{2n}x_n(i)^{c_{2n}-1} \\ \vdots & \vdots & \ddots & \vdots \\ a_{n1}c_{n1}x_1(i)^{c_{n1}-1} & a_{n2}c_{n2}x_2(i)^{c_{n2}-1} & \cdots & a_{nn} \end{pmatrix}. \tag{11}$$

Suppose $\sigma_1^{x(i)}$ is the minimum singular value of the Jacobian matrix $J(x(i))$ and δ is a given positive number. According to Lemma 1, we can get

$$\sigma_1^{x(i)} > \delta \tag{12}$$

if

$$|a_{kk}| > s_k + \delta \tag{13}$$

where $s_k = \max\{R_k, C_k\}$, and $R_k = \sum_{\substack{j=1 \\ j\neq k}}^{n} |a_{kj}c_{kj}x_k(i)^{c_{kj}-1}|$ and $C_k = \sum_{\substack{j=1 \\ j\neq k}}^{n} |a_{jk}c_{jk}x_k(i)^{c_{jk}-1}|$. From the definition of the nD-HCM, the observation state $x_k(i)$ satisfies that $0 \leq x_k(i) < N$. Thus

$$s_k + \delta < \max\left\{\sum_{\substack{j=1 \\ j\neq k}}^{n}\left|a_{kj}c_{kj}N^{c_{kj}-1}\right|, \sum_{\substack{j=1 \\ j\neq k}}^{n}\left|a_{jk}c_{jk}N^{c_{jk}-1}\right|\right\} + \delta.$$

Then, we can get that

$$\sigma_1^{x(i)} > \delta \tag{14}$$

if

$$|a_{kk}| > \max\left\{\sum_{\substack{j=1 \\ j\neq k}}^{n}\left|a_{kj}c_{kj}N^{c_{kj}-1}\right|, \sum_{\substack{j=1 \\ j\neq k}}^{n}\left|a_{jk}c_{jk}N^{c_{jk}-1}\right|\right\} + \delta. \tag{15}$$

Because $\sigma_1^{x(i)}$ is the minimum singular value of the Jacobian matrix $J(x(i))$, we can deduce that its n singular values are all greater than δ when the corresponding elements of the two parameter matrices A and C satisfy (15). Using this principle, one can construct these two parameter matrices. The detailed construction procedures for A and C with size $n \times n$ are described as follows.

1) *Step 1:* Set $k = 1$. Specify the value of the modular coefficient N and the lower bound of the n singular values for the Jacobian matrix of the nD-HCM, namely, δ.
2) *Step 2:* Set all off-diagonal elements in the kth row of matrix C to some random values.
3) *Step 3:* Set all off-diagonal elements in the kth row of matrix A to some random values.
4) *Step 4:* Set the absolute value of the kth principal diagonal element of A not smaller than $\max\{R_k, C_k\}+\delta$, where $R_k = \sum_{\substack{j=1 \\ j\neq k}}^{n} |a_{kj}c_{kj}N^{c_{kj}-1}|$ and $C_k = \sum_{\substack{j=1 \\ j\neq k}}^{n} |a_{jk}c_{jk}N^{c_{jk}-1}|$.
5) *Step 5:* Repeat steps 1–4 for $k = 2, 3, \ldots, n$.

Algorithm 1 shows the pseudocode of the aforementioned procedures for configuring A and C using inputs δ, a, c, and N, where $a = \{a_i\}_{i=1}^{n\cdot(n-1)}$ and $c = \{c_i\}_{i=1}^{n\cdot(n-1)}$ are the off-diagonal elements of A and C, δ is the lower bound of the n singular values of Jacobian matrix, and N is the modular coefficient of the chaotic map. The entity parameter matrix A and coefficient parameter matrix C configured using Algorithm 1 can make the generated nD-HCMs show expected dynamics and robust hyperchaotic behaviors.

Algorithm 1 Algorithm for Configuring the Parameter Matrices A and C

Input: $a = \{a_i\}_{i=1}^{n\cdot(n-1)}$, $c = \{c_i\}_{i=1}^{n\cdot(n-1)}$ and δ, where a_i and c_i are pseudo-random values, δ is a user-specified positive value.

Initialize $A = \mathbf{0}^{n\times n}$;
Initialize $C = \mathbf{0}^{n\times n}$;
for $k = 1$ to n **do**
  $C(k, k) = 1$;
  $C(k, 1{:}(k-1)) = \{c_i\}_{i=(k-1)\cdot(n-1)+1}^{(k-1)\cdot n}$;
  $C(k, (k+1){:}n) = \{c_i\}_{i=(k-1)\cdot n+1}^{k\cdot(n-1)}$;
  $A(k, 1{:}(k-1)) = \{a_i\}_{i=(k-1)\cdot(n-1)+1}^{(k-1)\cdot n}$;
  $A(k, (k+1){:}n) = \{a_i\}_{i=(k-1)\cdot n+1}^{k\cdot(n-1)}$;
  $A(k, k) = \max\{R_k, C_k\} + \delta + \theta$, where θ can any positive value and is set to 1 in this paper, $R_k = \sum_{\substack{j=1 \\ j\neq k}}^{n} |A(kj)C(kj)N^{C(kj)-1}|$ and $C_k = \sum_{\substack{j=1 \\ j\neq k}}^{n} |A(ji)C(kj)N^{C(jk)-1}|$;
end for

Output: the nD entity parameter matrix A and coefficient parameter matrix C.

C. Hyperchaotic Behavior Analysis

The chaotic behavior is a kind of disordered and irregular behaviors and it is highly sensitive to initial states, while the hyperchaotic behavior is a considerably more complex kind of behavior than the chaotic behavior. Many techniques have been developed to measure the existence of the chaos and hyperchaos. Among these techniques, the LE is a widely used and convinced criterion [37]. Here, we use it to study the dynamics of the proposed nD-HCM. A positive LE implies that the two close trajectories exponentially separate in each unit time and will result to be completely different behaviors eventually. An nD dynamic system has n LEs, and it will diverge in several directions with more than one positive LE. Thus, the dynamic properties of an nD dynamic system can be indicated by its number of positive LEs and their values [11]. The chaos in the sense of LE is described as Definition 2 [11].

Definition 2: For a dynamic system with globally bounded phase space, it has chaotic behavior if it has one positive LE and it has hyperchaotic behavior if it has more than one positive LE.

One can use Definition 2 to judge whether a dynamic system is chaotic or hyperchaotic. For an nD discrete chaotic map with initial value x_0, the n LEs of the system are calculated as

$$\mathrm{LE}_k = \lim_{t\to\infty} \frac{1}{t} \ln(\lambda_k), \quad k = 1, 2, \ldots, n \tag{16}$$

where λ_k is the kth eigenvalue of the matrix J_t, and J_t is the multiplications of the Jacobian matrix of the dynamic map at each iteration time, namely, $J_t = J(x_0)J(x_1)\cdots J(x_{t-1})$.

Before analyzing the hyperchaotic behavior of the generated nD-HCM, we present Theorem 2 that describes the relationship between the singular values of the multiplication result of matrices with the singular values of every matrix.

Theorem 2 [38]: Let $0 \le \sigma_1^{(1)} \le \sigma_2^{(1)} \le \cdots \le \sigma_n^{(1)}$, $0 \le \sigma_1^{(2)} \le \sigma_2^{(2)} \le \cdots \le \sigma_n^{(2)}$, $\cdots$, $0 \le \sigma_1^{(t)} \le \sigma_2^{(t)} \le \cdots \le \sigma_n^{(t)}$ be the n singular values of the matrix $\mathbf{P_1}, \mathbf{P_2}, \ldots, \mathbf{P_t} \in \mathbb{R}^{\mathbf{n}\times\mathbf{n}}$, respectively. The n singular values of the matrix $\mathbf{Q} = \mathbf{P_1}\mathbf{P_2}\cdots\mathbf{P_t}$, $\sigma_1, \sigma_2, \cdots, \sigma_n$, satisfy that

$$\sigma_k \ge \sigma_1^{(1)}\sigma_1^{(2)}, \ldots \sigma_1^{(t)} \tag{17}$$

and

$$\sigma_k \le \sigma_n^{(1)}\sigma_n^{(2)}, \ldots \sigma_n^{(t)} \tag{18}$$

where $k = 1, 2, \ldots, n$.

Proposition 1 states that the proposed nD-HCM has hyperchaotic behaviors when its parameters satisfy some requirements.

Proposition 1: The nD-HCM in (7) with nD parameter matrices A and C configured by Algorithm 1 has hyperchaotic behavior if the parameter $\delta \ge 1$.

Proof: Because the modular operation is a bounded operator, the phase space of the nD-HCM in (7) is always globally bounded. That is, the first condition of Definition 2 is satisfied.

The multiplication of the Jacobian matrices of the nD-HCM in (7) from iteration time 0 to iteration time $t-1$ can be written by

$$J_t = J(x_0)J(x_1)\cdots J(x_{t-1}). \tag{19}$$

Suppose $0 \le \sigma_1^{x(i)} \le \sigma_2^{x(i)} \le \cdots \le \sigma_n^{x(i)}$ are the n singular values of $J(x_i)$, and $0 \le \sigma_1 \le \sigma_2 \le \cdots \le \sigma_n$ are the n singular values of J_t. Because the parameter matrices A and C are configured by Algorithm 1 following the constraint of (15), the minimum singular value of the Jacobian matrix $J(x(i))$ satisfying (14), that is, $\sigma_1^{x(i)} > \delta$.

From (17) of Theorem 2, one can get that

$$\sigma_k \ge \sigma_1^{x(0)}\sigma_1^{x(1)}\cdots\sigma_1^{x(t-1)} > \delta^t$$

where $k = 1, 2, \ldots, n$. Thus, the minimum singular value σ_1 of the matrix J_t is larger than δ^t.

According to the preliminaries in linear algebra, the relationship between the singular values and eigenvalues of an square matrix $D \in \mathbb{R}^{n\times n}$ satisfies the following inequality:

$$\sigma_1(D) \le |\lambda_k(D)| \le \sigma_n(D) \tag{20}$$

where $k = 1, 2, \ldots, n$, $\sigma_1(D)$ and $\sigma_n(D)$ denote the minimum and maximum singular values of D, respectively, and $\lambda_k(D)$ is the kth eigenvalue.

Since the minimum singular value of the matrix J_t is larger than δ^t, we can get that

$$|\lambda_k| > \delta^t, \quad k = 1, 2, \ldots, n \tag{21}$$

where λ_k denotes the kth eigenvalue of J_t. From (16), the n LEs of the nD-HCM in (7) are estimated as

$$\mathrm{LE}_k > \lim_{t\to\infty} \frac{1}{t}\ln\left(\delta^t\right) = \ln(\delta) \tag{22}$$

where $k = 1, 2, \ldots, n$. It is worth noting that if the eigenvalue $\lambda_k < 0$, the calculated LE is a complex number and the final LE value is the real part of the complex number [39].

Because the parameter $\delta \ge 1$, $\mathrm{LE}_k > 0$ for $k = 1, 2, \ldots, n$, the generated nD-HCM has n positive LEs. Therefore, the generated nD-HCM can exhibit chaotic behavior when the dimension n is greater than or equal to 1, and exhibit hyperchaotic behavior when n is greater than or equal to 2. ■

Proposition 1 tells the constraint conditions of the generated nD-HCM in showing hyperchaotic behavior. By specifying an arbitrary positive δ in configuring the parameter matrices A and C, one can limit the lower bound of all the LEs of the generated nD-HCM, and ensure that it shows expected properties and robust hyperchaotic behaviors.

IV. Illustrative Examples

Two examples of nD-HCM are generated to verify the effect of the proposed method: 1) a 3D-HCM and 2) a 9D-HCM. According to Proposition 1 and the parameter configuring procedure in Algorithm 1, the elements in sequences a and c can be set as any values and δ should be not smaller than 1. In our examples, the elements in a are randomly fetched from data set $\{1, 2, \ldots, 10\}$, the elements in c are randomly fetched from data set $\{1, 2, \ldots, 5\}$, the δ is set to $\delta = 1$, and the modular coefficient is set to $N = 1$. One has great flexibility to specify those parameters as other values.

A. 3D-HCM

When generating a 3D-HCM, a 3-D entity parameter matrix A and a 3-D coefficient parameter matrix C should be configured. The sequences a and c should have six elements. Suppose these randomly generated parameters are $a = \{1, 3, 10, 4, 5, 3\}$ and $c = \{2, 5, 4, 5, 3, 3\}$, and set $\delta = 1$. According to Algorithm 1, the matrices A and C can be generated as

$$A = \begin{pmatrix} 57 & 1 & 3 \\ 10 & 62 & 4 \\ 5 & 3 & 37 \end{pmatrix} \text{ and } C = \begin{pmatrix} 1 & 2 & 5 \\ 4 & 1 & 5 \\ 3 & 3 & 1 \end{pmatrix} \tag{23}$$

respectively. Setting the modular coefficient as one, a 3D-HCM can be generated as

$$\begin{cases} x_1(i+1) = 57x_1(i) + x_2(i)^2 + 3x_3(i)^5 \mod 1 \\ x_2(i+1) = 10x_1(i)^4 + 62x_2(i) + 4x_3(i)^5 \mod 1 \\ x_3(i+1) = 5x_1(i)^3 + 3x_2(i)^3 + 37x_3(i) \mod 1. \end{cases} \tag{24}$$

Since the singular values of its Jacobian matrix at each iteration time are all larger than one, according to Theorem 2, all the eigenvalues of the multiplication of these Jacobian matrices are larger than one. This ensures that all the LEs of the 3D-HCM are positive. Using the well-known Wolf's algorithm, we can calculate out that the three LEs of the 3D-HCM are $\mathrm{LE}_1 = 4.1707$, $\mathrm{LE}_2 = 4.0138$, and $\mathrm{LE}_3 = 3.5799$. This experimentally indicates that the generated 3D-HCM has three positive LEs and thus shows hyperchaotic behaviors.

Chaos is studied in the mathematical domain with infinite precision. When a chaotic system is implemented in digital platforms with finite precision, its chaotic behavior will degrade to regular behavior due to the precision truncation [40]. Since all the researches and applications about chaos are performed on digital platforms, it is important to

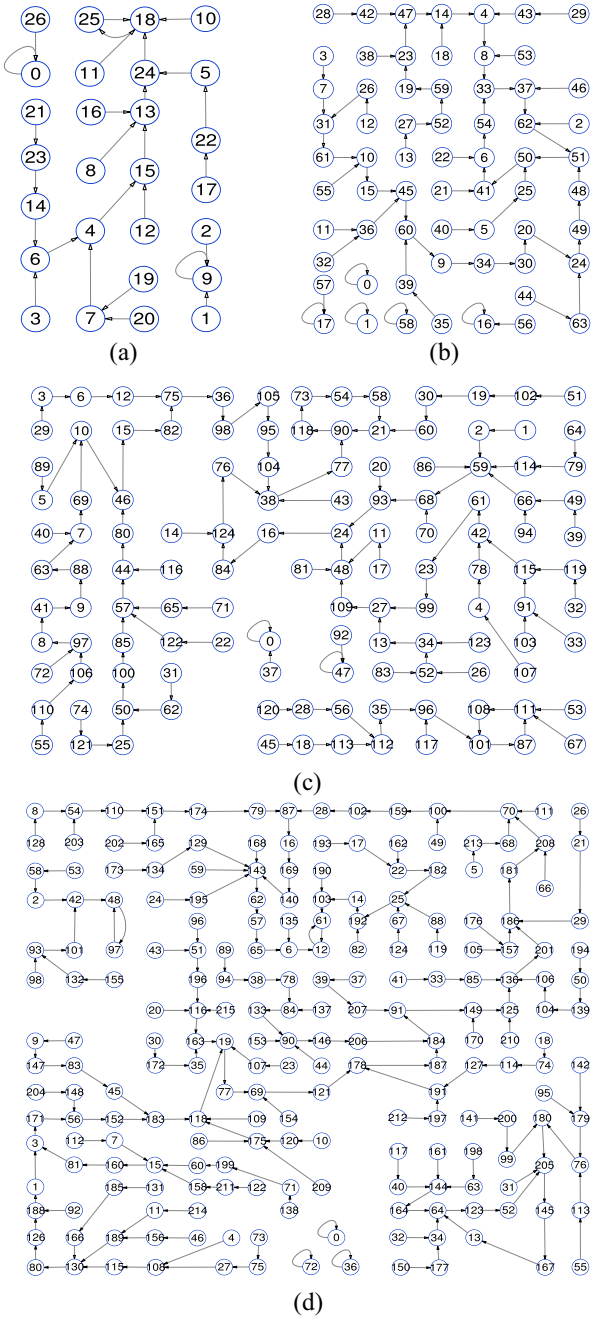

Fig. 2. State mapping networks of the 3D-HCM with various fixed precisions. (a) $m = 3$. (b) $m = 4$. (c) $m = 5$. (d) $m = 6$.

study the properties of a chaotic system in the digital domain. Here, we apply the state-mapping network [40], [41] to analyze the properties of the 3D-HCM in the fixed-point domain. Since the inputs and outputs of the 3D-HCM are all within the range $[0, 1)$, we set the arithmetic precision as $1/m$, and the fixed points in the interval $[0, 1)$ can be represented as $\{0, 1/m, \ldots, (m-1)/m\}$. Thus, each dimension has m possible states, and each observation state of the 3D-HCM has m^3 possible states. To facilitate the generation of a state-mapping network, we convert each observation state $x = [x_1, x_2, x_3]$ to be an integer j using the following formula:

$$j = F(x) = R(mx_1) + R(mx_2) \times m + R(mx_3) \times m^2 \quad (25)$$

where $R(\cdot)$ is the round quantization function. Obviously, $j \in \{0, 1, \ldots, m^3 - 1\}$. Suppose that x' denotes the output of the 3D-HCM with input x, $j = F(x)$, and $k = F(x')$, then a directed line can be drawn from the node j to node k. After connecting all the m^3 input nodes with their corresponding output nodes using directed lines, the state-mapping network can be generated. Fig. 2 depicts the state-mapping networks of the 3D-HCM under various fixed precisions $m = \{3, 4, 5, 6\}$. As can be seen, these state-mapping networks have some obvious characteristics.

1) All the nodes are weakly connected. The largest subgraphs contain a path, which is linked to two arbitrary nodes k and j in the underlying undirected version of the subgraph.
2) Each weakly linked node has only one out-degree or self-loop, and the node with value zero is always self-looping.
3) The sizes of the largest subgraph can occupy more than half of the whole networks, and their sizes sharply grow as the precision increases.

These phenomena show the complex dynamic properties of the 3D-HCM in the digital domain.

B. 9D-HCM

When $n = 9$, a 9-D entity parameter matrix A and a 9-D coefficient parameter matrix C should be configured. The parameters are generated using the same method with them in the 3D-HCM. Then, two data sequences $a = \{a_i\}_{i=1}^{72}$ and $c = \{c_i\}_{i=1}^{72}$ are randomly generated, where a_i are randomly fetched from data set $\{1, 2, \ldots, 10\}$ and c_i are randomly fetched from data set $\{1, 2, \ldots, 5\}$. δ is set to $\delta = 1$. Using Algorithm 1, the parameter matrices A and C of the 9D-HCM can be produced as

$$A = \begin{pmatrix} 175 & 5 & 10 & 1 & 2 & 3 & 10 & 1 & 6 \\ 5 & 177 & 1 & 3 & 5 & 10 & 8 & 5 & 7 \\ 5 & 5 & 123 & 4 & 2 & 6 & 8 & 8 & 5 \\ 10 & 8 & 2 & 128 & 6 & 5 & 1 & 6 & 8 \\ 4 & 4 & 1 & 9 & 104 & 3 & 4 & 2 & 7 \\ 6 & 9 & 9 & 10 & 8 & 155 & 10 & 2 & 1 \\ 6 & 8 & 6 & 6 & 7 & 10 & 191 & 10 & 8 \\ 4 & 9 & 6 & 9 & 6 & 9 & 4 & 162 & 3 \\ 10 & 3 & 2 & 9 & 2 & 9 & 6 & 8 & 193 \end{pmatrix} \quad (26)$$

and

$$C = \begin{pmatrix} 1 & 4 & 4 & 1 & 3 & 4 & 5 & 1 & 4 \\ 3 & 1 & 1 & 4 & 1 & 1 & 3 & 1 & 2 \\ 4 & 1 & 1 & 1 & 4 & 1 & 4 & 2 & 5 \\ 1 & 4 & 1 & 1 & 2 & 2 & 5 & 2 & 3 \\ 2 & 2 & 1 & 5 & 1 & 3 & 5 & 2 & 1 \\ 5 & 4 & 3 & 1 & 3 & 1 & 2 & 2 & 2 \\ 5 & 4 & 2 & 3 & 3 & 2 & 1 & 4 & 2 \\ 5 & 3 & 5 & 3 & 2 & 3 & 2 & 1 & 3 \\ 4 & 5 & 4 & 1 & 5 & 5 & 4 & 5 & 1 \end{pmatrix}$$

respectively. When setting the modular coefficient $N = 1$ in (7), a 9D-HCM can be generated. By calculation, the nine LEs of the 9D-HCM are $\mathrm{LE}_1 = 5.3882$, $\mathrm{LE}_2 = 5.2191$,

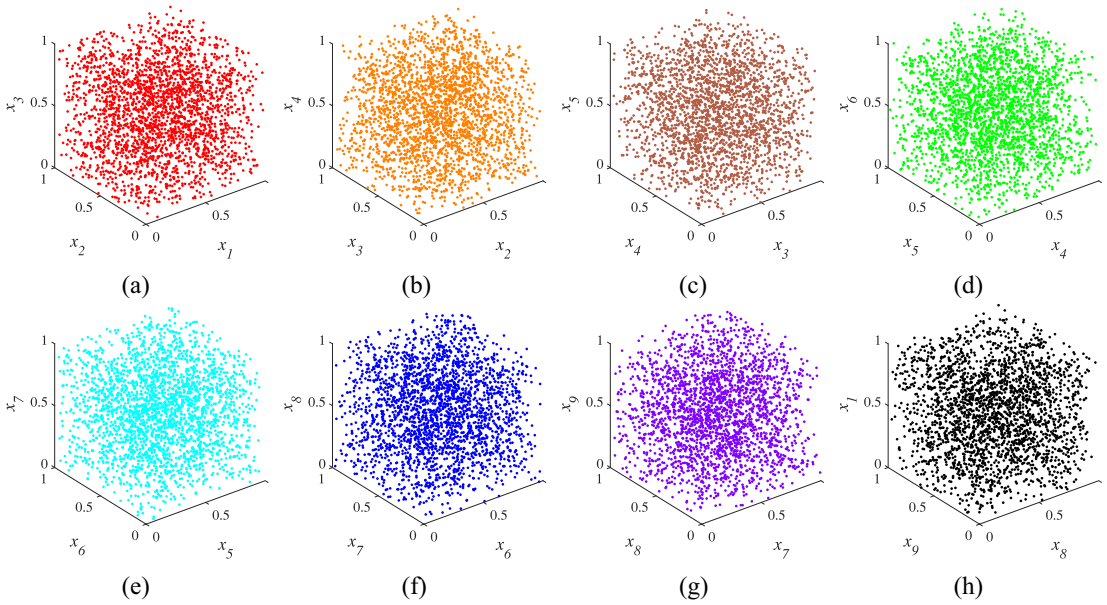

Fig. 3. Hyperchaotic trajectories of the generated 9D-HCM with 2000 states in various 3-D phase spaces. (a) $x_1 - x_2 - x_3$ space. (b) $x_2 - x_3 - x_4$ space. (c) $x_3 - x_4 - x_5$ space. (d) $x_4 - x_5 - x_6$ space. (e) $x_5 - x_6 - x_7$ space. (f) $x_6 - x_7 - x_8$ space. (g) $x_7 - x_8 - x_9$ space. (h) $x_8 - x_9 - x_1$ space.

$\mathrm{LE}_3 = 5.1514$, $\mathrm{LE}_4 = 5.1304$, $\mathrm{LE}_5 = 5.0805$, $\mathrm{LE}_6 = 5.0137$, $\mathrm{LE}_7 = 4.8382$, $\mathrm{LE}_8 = 4.7964$, and $\mathrm{LE}_9 = 4.6336$. Obviously, the nine LEs of the 9D-HCM are all positive, indicating that it owns hyperchaotic behaviors.

To test the randomness of the 9D-HCM, we generate its trajectory by setting the number of states as 2000 and initial state as $x(0) = \mathbf{0.1}_{9\times 1}$. Fig. 3 plots the distributions of its trajectory when being projected in various 3-D phase spaces. It is clear that the outputted trajectory of the 9D-HCM is uniformly distributed in each 3-D phase space, which demonstrates that the 9D-HCM's outputs have good randomness.

V. Performance Analysis

In this section, we analyze the performance of the proposed nD-HCM using the indicators of LE, correlation dimension [42], joint entropy [43], and time complexity. For our proposed nD-HCM, when generating the parameter matrices A and C in Algorithm 1, all elements of date sequences a and c are randomly fetched from integer sets $\{1, 2, \ldots, 10\}$ and $\{1, 2, \ldots, 5\}$, respectively. To show the superiority of the proposed method, this section compares it with several HD chaotic map generation methods, including Shen's method [33], Chen's method [11], Zhang's method [44], and Natiq's method [45], and several 3-D chaotic maps, including Saljoughi's map [27], Filali's map [28], Lai's system [29], and Li's map [46].

In the comparison experiments, a large number of HD chaotic maps with different dimensions are required. However, for some of these competing HD chaotic map generation methods, the literatures only provide several examples of HD chaotic maps with certain dimensions. When generating chaotic maps with different dimensions, these provided parameters cannot achieve the properties expected in literatures, and thus their values should be adjusted. To obtain a fair comparison result, the experiments set the parameters in all the HD chaotic map generation methods following the below rules.

1) If the parameter values provided in the literatures can obtain arbitrary dimensional chaotic map with expected properties, we directly apply these parameter values.
2) If the provided parameter values hardly obtain HD chaotic maps with expected properties for some dimensions, we adjust their parameters to make sure that the produced HD chaotic maps can exhibit the properties reported in the original literature.
3) Under the condition that the produced HD chaotic maps can show the properties reported in the original literature, we adjust the parameter values to the same level as the proposed method in all chaotic map generation methods.

As a consequence, the parameter values in Shen's method are set to $a = -0.1$ and $\epsilon \in [1, 10]$, in Chen's method are set to $\epsilon \in [4, 10]$ and $\sigma = 0.01$, in Zhang's method are set to $b \in (0, 6]$, and in Natiq's method are set to $\beta = 5$, $\sigma = 1.5\pi$, and $\mu \in [1, 10]$. When generating an nD chaotic map, the parameters in these generation methods are randomly fetched from their respective intervals. For the competing 3-D chaotic maps, their parameters are set the same as those in the original literature.

A. Lyapunov Exponent

From Definition 2, a nonlinear system with global bound shows chaotic behavior if it possesses one positive LE and it shows hyperchaotic behavior if it possesses more than one positive LE. Because the LE characterizes the separation rate of two trajectories of a nonlinear system beginning from extremely near initial values, the chaos complexity of a nonlinear system can be indicated by its largest LE (LgtLE)

TABLE I
LEs OF DIFFERENT 3-D CHAOTIC MAPS

	LE_1	LE_2	LE_3	Positive No.
Saljoughi's [27]	0.0240	0.0238	0.0230	3
Filali's [28]	0.2112	0.1883	-2.7021	2
Lai's [29]	0.3112	0.0000	-1.2453	1
Li's [46]	0.0801	0.0126	-0.5513	2
Shen's [33]	0.8094	0.0000	-1.1088	1
Chen's [11]	0.8607	0.8607	0.5137	3
Zhang's [44]	0.9096	0.9070	0.9031	3
Natiq's [45]	2.2168	0.2603	-0.2014	2.18
nD-HCM	**4.0269**	**3.6465**	**3.3669**	**3**

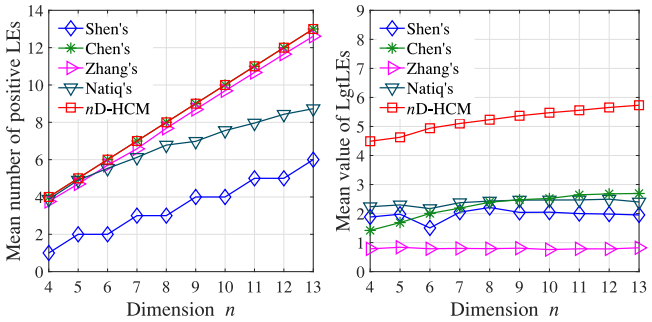

Fig. 4. LEs of 100 nD chaotic maps produced by various methods under various dimensions $n \in \{4, 5, \ldots, 13\}$. (a) Mean number of positive LEs. (b) Mean LgtLEs.

TABLE II
CDs OF DIFFERENT 3-D CHAOTIC MAPS

	CD_1	CD_2	CD_3
Saljoughi's [27]	0.6812	0.6812	0.6812
Filali's [28]	1.9048	1.9028	1.9031
Lai's [29]	1.2915	1.2801	1.2010
Li's [46]	1.7429	1.7438	1.7446
Shen's [33]	1.4853	1.4786	1.5072
Chen's [11]	0.1262	0.3393	0.4406
Zhang's [44]	1.5029	1.5046	1.5025
Natiq's [45]	1.4523	1.4593	1.4528
nD-HCM	**1.9764**	**1.9721**	**1.9683**

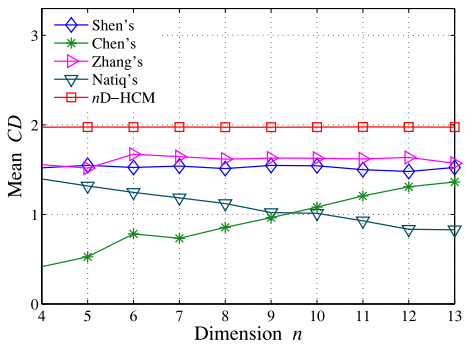

Fig. 5. Mean CDs of nD chaotic maps produced by various methods under different dimensions $n \in \{4, 5, \ldots, 13\}$.

and the number of positive LEs, according to the discussions in [31].

Two sets of experiments are designed to evaluate the performance of different chaotic maps using LE. The first set measures the LEs of 3-D chaotic maps. For each chaotic map generation method, we randomly generate 100 3-D chaotic maps and calculate the mean number of positive LEs. The three LEs of different 3-D chaotic maps are listed in Table I. Because the 3-D chaotic maps generated by Natiq's method [45] have different numbers of positive LEs, the mean number is decimal. Saljoughi's chaotic map [27] and the 3-D chaotic maps produced by Chen's method [11], Zhang's method [44] and our method can achieve three positive LEs. Nevertheless, the three LEs of 3-D chaotic maps produced by the proposed method are all greater than the LEs of other 3-D chaotic maps.

The second set of experiments tests the LEs of the five HD chaotic map generation methods under different map dimensions $n \in \{4, 5, \ldots, 13\}$. For each generation method in each dimension, we randomly generate 100 nD chaotic maps and calculate the mean numbers of positive LEs and mean LgtLEs. Fig. 4 shows the LEs of the nD chaotic maps produced by each method under various dimensions. As shown in Fig. 4(a), the nD chaotic maps produced by our method and Chen's method [11] have n positive LEs, which reach the maximum number. In contrast, the nD chaotic systems produced by Shen's method [33] have $\lfloor n-1 \rfloor/2$ positive LEs, and produced by Zhang's method [44] and Natiq's method [45] have changeable numbers of positive LEs. From Fig. 4(b), we can see that although our method and Chen's method [11] produce nD chaotic maps with the same number of positive LEs, the chaotic maps produced by our proposed method have much larger LgtLEs than the chaotic maps produced by the existing methods. This demonstrates that the HCMs produced by our method have complex dynamic behaviors.

B. Correlation Dimension

The CD is a kind of fractal dimension that tests the space dimensionality occupied by a chaotic sequence. A nonlinear system has strange attractors if it has a positive CD and a larger CD means occupying a larger space dimensionality, which further implies the higher strangeness of the strange attractor.

The experiment settings are the same as in the LE experiment. First, the CDs of the three time series generated from different 3-D chaotic maps are calculated and listed in Table II. One can see that the 3-D chaotic map produced by our method owns the biggest CDs. Besides, we test the CDs of the five chaotic map generation methods under map dimensions $n \in \{4, 5, \ldots, 13\}$. To get a stable result, 100 nD chaotic maps are randomly produced by each method and the final CD denotes the mean value of the n CDs for n chaotic sequences. Fig. 5 depicts the mean CDs of the chaotic maps produced by each method under different dimensions. One can see that our method produces HD chaotic maps with the largest mean CDs. This indicates that our method can produce HD chaotic maps with higher strange attractors.

C. Joint Entropy

The JE is used to characterize the uncertainty and randomness of a set of signals. Since the state space of an nD chaotic system has n dimensions, namely, $x(i) = \{x_1(i),$

TABLE III
MAXIMUM JES OF 100 3-D CHAOTIC MAPS PRODUCED BY VARIOUS CHAOTIC MAP GENERATION METHODS WITH VARIOUS NUMBERS OF INTERVALS I

	Number of intervals I												
	3	5	7	9	11	13	15	17	19	21	23	25	27
Shen's [33]	3.6069	5.8057	6.4996	7.8524	8.5350	9.3009	9.7152	10.1124	10.5413	10.9352	11.1773	11.5626	11.7711
Chen's [11]	0.3241	1.6264	2.3375	2.3455	3.0157	3.5323	3.5689	4.0288	4.2918	4.5146	4.8105	5.1563	5.3773
Zhang's [44]	4.6271	6.7167	8.0650	9.0904	9.9105	10.6603	11.2033	11.8006	12.2514	12.6057	13.0559	13.3889	13.7038
Natiq's [45]	4.3341	6.2640	7.5652	8.5340	9.3094	9.9700	10.5502	11.0092	11.4182	11.7787	12.1019	12.4009	12.6923
nD-HCM	**4.7255**	**6.9465**	**8.4101**	**9.5020**	**10.3729**	**11.0974**	**11.7177**	**12.2600**	**12.7419**	**13.1754**	**13.5694**	**13.9304**	**14.2637**
$JE_{\max}$	4.7549	6.9658	8.4221	9.5098	10.3783	11.1013	11.7207	12.2624	12.7438	13.1770	13.5707	13.9316	14.2647

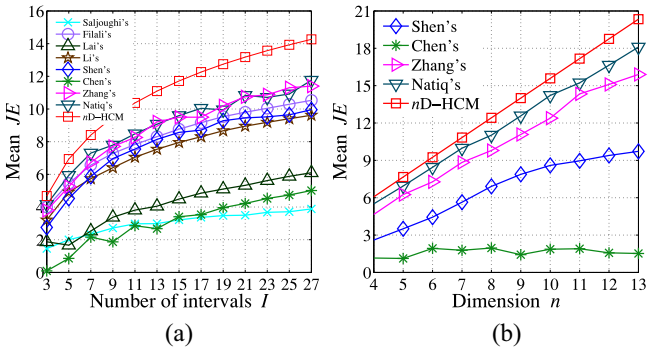

Fig. 6. JE results of different chaotic maps. (a) JEs of four 3-D chaotic maps and the mean JEs of 100 3-D chaotic maps produced by five generation methods under various number of intervals $I \in \{3, 5, \ldots, 27\}$. (b) Mean JEs of 100 nD chaotic maps under different map dimensions $n \in \{4, 5, \ldots, 13\}$ by setting the number of intervals $I = 3$.

TABLE IV
MAXIMUM JES OF 100 nD CHAOTIC MAPS PRODUCED BY EACH METHOD UNDER MAP DIMENSIONS $n \in \{4, 5, \ldots, 13\}$ BY SETTING THE NUMBER OF INTERVALS $I = 3$

n	**HD chaotic map generation methods**					$JE_{\max}$
	Shen's [33]	Chen's [11]	Zhang's [44]	Natiq's [45]	nD-HCM	
4	3.5819	1.4637	5.9805	5.7236	**6.1746**	6.3399
5	4.6441	1.3297	7.5045	7.2192	**7.7191**	7.9248
6	5.5444	2.0713	8.9699	8.6995	**9.2702**	9.5098
7	6.4781	2.3112	10.5170	10.1322	**10.8551**	11.0947
8	7.7241	2.2244	12.0447	11.5996	**12.4259**	12.6797
9	8.9073	1.5767	13.6005	13.0824	**14.0079**	14.2647
10	10.0498	1.9285	15.0882	14.5328	**15.5899**	15.8496
11	11.3156	2.3983	16.6424	15.9788	**17.1779**	17.4346
12	12.5194	2.0964	18.2022	17.4303	**18.7601**	19.0196
13	13.4677	1.9397	19.6338	18.8651	**20.3425**	20.6045

$x_2(i), \ldots, x_n(i)\}^T \in R^{n\times 1}$, the system has n signals, namely, $x_1, x_2, \cdots, x_n$, where $x_j = \{x_j(1), x_j(2), \ldots, x_j(i), \ldots, \}$. When uniformly separating each signal into I intervals, the JE of the n signals of an nD chaotic system is defined as

$$\mathrm{JE} = -\sum_{k_1}^{I}\sum_{k_2}^{I}\cdots\sum_{k_n}^{I} P\left(b_{k_1}b_{k_2}\ldots b_{k_n}\right) \log_2 P\left(b_{k_1}b_{k_2}\ldots b_{k_n}\right) \tag{27}$$

where $P(b_{k_1}b_{k_2}\ldots b_{k_n})$ denotes the joint probability of the k_1th state in the first interval, k_2th state in the second interval, $\cdots$, k_nth state in the nth interval. Obviously, the JE takes a positive value, and its theoretical maximum score can be obtained when the n signals are complete uncertainty, namely, $P(b_{k_1}b_{k_2}\ldots b_{k_n}) = P(b_{k_1})P(b_{k_2})\cdots P(b_{k_n})$ and $P(b_{k_1}) = P(b_{k_2}) = \cdots = P(b_{k_n}) = 1/I$. Thus, the maximum JE is calculated as

$$\mathrm{JE}_{\max} = n\log_2(I). \tag{28}$$

Thus, an actual JE satisfies that $0 \le \mathrm{JE} \le n\log_2(I)$, and a higher JE shows better uncertainty of the n signals.

Two groups of experiments are applied to compute the JEs of the outputted signals generated by various chaotic maps. The first group fixes the dimension $n = 3$ and tests the JEs under the number of intervals $I \in \{3, 5, \ldots, 27\}$. The three signals of each 3-D chaotic map with length I^5 are generated and their JEs are calculated. For each nD chaotic map generation method, randomly generate 100 3-D chaotic maps and the mean value of these 3-D chaotic maps is calculated. Fig. 6(a) plots the JEs of four 3-D chaotic maps and the mean JEs of the 3-D chaotic maps produced by each generation method. As shown that the 3-D chaotic map produced by our method owns the largest mean JEs. Table III lists the maximum JEs of the 100 3D chaotic maps produced by each generation method under various numbers of intervals. It is clear that our method can produce 3-D chaotic maps with the largest JEs, and their maximum JEs approach to the theoretical maximum ones.

The other group of experiments is performed to analyze the JEs under various dimensions $n \in \{4, 5, \ldots, 13\}$ by setting the number of intervals $I = 3$. For each chaotic map generation method under various dimensions n, we randomly generate 100 nD chaotic maps. Then the n signals with length 3^{n+1} are generated by each nD chaotic map and their JE is calculated. Fig. 6(b) shows the mean JEs of these 100 nD chaotic maps generated by each method. It can be observed that the nD chaotic maps produced by our method achieve larger mean JEs than the nD chaotic maps produced by other methods. The maximum JEs of the 100 nD chaotic maps are listed in Table IV. One can see that the maximum JEs of the chaotic maps generated by our method are also conspicuously greater than that of the chaotic maps generated by the existing methods, and are extremely approach to the theoretical maximum values. This demonstrates that our method can produce HD chaotic maps with high uncertainty and randomness.

D. Complexity Analysis

The time complexity is an important indicator to evaluate the ability of an nD chaotic map in practical applications. The chaotic maps generated by all the competing and our methods involve the following operations: addition, multiplication, division, modular, and trigonometric function. For our

TABLE V
NUMBERS OF DIFFERENT OPERATIONS THAT REQUIRED BY DIFFERENT nD CHAOTIC MAPS IN ONE-TIME ITERATION AND THE ACTUAL TIME COSTS (SECOND) OF GENERATING CHAOTIC SEQUENCES WITH LENGTH 10^8 BY EACH nD CHAOTIC MAP USING C PROGRAMMING LANGUAGE

		nD chaotic map generation methods				
		Shen's [33]	Chen's [11]	Zhang's [44]	Natiq's [45]	nD-HCM
Number of operation	Addition	$14n$	$3n(n-1)/2$	0	0	$\boldsymbol{n^2-n}$
	Multiplication	$23n$	$3/2n^2-1/2n$	n	$2n-1$	$\boldsymbol{2n^2-n}$
	Division	n	0	0	1	**0**
	Modular	0	$n(n-1)/2$	0	0	$\boldsymbol{n}$
	Trigonometric function	$4n$	0	$2n$	n	**0**
Actual time costs	3D	14.974	7.980	14.671	4.399	**5.085**
	4D	18.154	13.185	19.048	5.621	**8.147**
	5D	24.664	20.122	22.198	7.362	**12.146**
	6D	31.173	27.770	26.730	8.817	**18.420**
	7D	38.371	37.327	31.330	10.144	**25.710**
	8D	41.847	48.349	36.343	11.767	**34.569**
	9D	49.381	62.054	40.828	12.892	**43.118**
	10D	55.749	75.321	46.115	14.124	**51.413**

method, the nondiagonal elements of the parameter matrix C can be any positive integer and we set them as 2 for simplicity. Since the chaotic systems generated by Shen's [33] method are continuous, we should first discretize these systems and use the fourth-order Runge–Kutta algorithm to discretize the continuous systems.

Table V lists the numbers of different operations that are required by different nD chaotic maps in one-time iteration. As can be seen, Chen's [11] and our methods have the $O(n^2)$ degree of basic operations (e.g., addition, multiplication, division, and modular), while Shen's [33], Zhang's [44], and Natiq's [45] methods have the $O(n)$ degree of basic operations. However, Shen's [33], Zhang's [44], and Natiq's [45] methods have $O(n)$ degree of time-consuming trigonometric operation, while Chen's [11] and our methods do not have. Table V also lists the actual time costs of generating chaotic sequences with length 10^8 by each nD chaotic map using C programming language. As shown that the time costs of all the chaotic maps have the same order of magnitude. As a result, the nD chaotic maps generated by our method have the same magnitude of time costs with that generated by state-of-the-art methods. However, they can show much better performance indicators.

VI. SECURE COMMUNICATION

The differential chaos shift keying (DCSK) is a typical kind of chaos-based secure communication scheme, and it can well balance the tradeoff between the bit error ratio (BER) and implementation cost [47]. When a chaotic system is used to transmit data, the distribution of its trajectory can significantly affect the performance of the communication system to resist channel noise. Because our nD-HCMs can produce more uniformly distributed chaotic outputs than existing chaotic maps, they can show better performance in resisting channel noise. This section develops a new DCSK to evaluate the performance of various chaotic maps in the secure communication application.

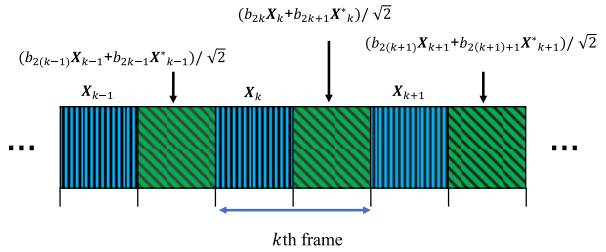

Fig. 7. Transmitted signal in the proposed DCSK.

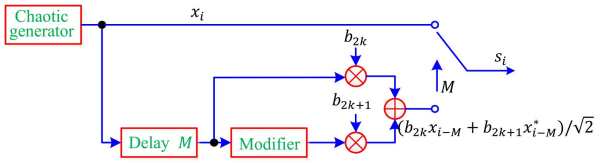

Fig. 8. Transmitter of the proposed DCSK.

A. Communication Scheme

The proposed DCSK includes two components: 1) transmitter and 2) receiver. The following contents detail the structures of the transmitter and receiver.

1) Transmitter: The transmitted signal can be generated by coding the transmitted data with the chaotic sequences and its structure is shown in Fig. 7. Each frame in the signal includes a reference signal and an information signal. For the kth frame, the reference signal $\mathbf{X}_k$ is an M-length chaotic sequence, where $\mathbf{X}_k = \{x_i | 2kM < i \le (2k+1)M\}$ and M denotes a spreading factor. The information signal is the sum of two parts, where the first part is the multiplication of $\mathbf{X}_k$ with data bit b_{2k}, and the other part is the multiplication of the modified reference signal $\mathbf{X}_k{}^*$ with data bit b_{2k+1}. The modified reference signal $\mathbf{X}_k{}^*$ is generated from the reference signal $\mathbf{X}_k$, where its former $M/2$ elements are the elements in the odd positions of $\mathbf{X}_k$, and its latter $M/2$ elements are the elements in the even positions of $\mathbf{X}_k$. The modified reference signal $\mathbf{X}_k{}^*$ in the k-frame can be written as

$$\mathbf{X}_i{}^* = \begin{cases} \mathbf{X}_{2(i-kM)-1}, & 2kM < i \le 2kM + M/2 \\ \mathbf{X}_{2(i-kM-M/2)}, & 2kM + M/2 < i \le (2k+1)M. \end{cases} \tag{29}$$

Fig. 8 plots the block diagram of the transmitter structure in the proposed DCSK. When generating the kth frame of the transmitted signal, a chaotic sequence $\mathbf{X}_k$ with length M is produced by a chaotic map. After the time delay block, the system has two branches in the second time slot of the kth frame. The first data bit b_{2k} is modulated by the delayed reference signal $\mathbf{X}_{i-M}$ in the first branch, and the second data bit b_{2k+1} is modulated with the modified reference signal $\mathbf{X}^*_{i-M}$, which is generated by the modifier component. Then, the kth frame in the transmitted signal s_i can be expressed by

$$s_i = \begin{cases} x_i, & 2kM < i \le (2k+1)M \\ \left(b_{2k}x_{i-M} + b_{2k+1}x_{2(i-kM-M)-1}\right)/\sqrt{2} & \\ & (2k+1)M < i \le 2kM + 3/2M \\ \left(b_{2k}x_{i-M} + b_{2k+1}x_{2(i-kM-3/2M)}\right)/\sqrt{2} & \\ & 2kM + 3/2M < i \le 2(k+1)M. \end{cases}$$

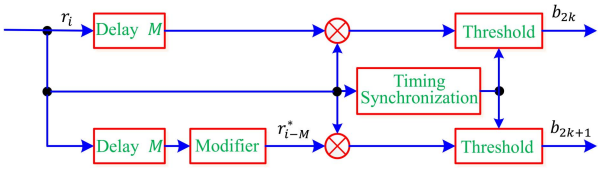

Fig. 9. Receiver of the proposed DCSK.

2) Receiver: When receiving the transmitted signal, the receiver demodulates the signal and its structure is depicted in Fig. 9. Due to the transmission noise, the received signal r_i is different from the transmitted signal s_i and it undergoes a delay block unit and modifier block unit. The modifier component is to change the signal r_i into signal $r_i{}^*$ by performing the same operation as in (29). The two branches in the receiver can concurrently demodulate the two data bits in each frame.

To exact the data bits, the received signal r_i is multiplied with its delay versions r_{i-M} and $r_{i-M}{}^*$ on the two branches. Thus, the correlators for the two bits b_{2k} and b_{2k+1} are

$$Z_{2k} = \sum_{i=(2k+1)M+1}^{2(k+1)M} r_i r_{i-M} \tag{30}$$

$$Z_{2k+1} = \sum_{i=(2k+1)M+1}^{2(k+1)M} r_i r^*_{i-M} \tag{31}$$

respectively. Because of the transmission noise, the received signal can be presented as $r_i = x_i + \xi_i$, where ξ_i denotes the added noise. Then, the correlators for the data bits b_{2k} and b_{2k+1} can be calculated as

$$Z_{2k} = \frac{\sqrt{2}}{2} \sum_{i=(2k+1)M+1}^{2(k+1)M} b_{2k} x^2_{i-M} + \Phi \tag{32}$$

$$Z_{2k+1} = \frac{\sqrt{2}}{2} \sum_{i=(2k+1)M+1}^{2(k+1)M} b_{2k+1} x^2_{i-M} + \Psi \tag{33}$$

respectively, where Φ and Ψ are the noise parts. The detailed representations of Φ and Ψ can be referred to the Appendix. Because the energy of the noise is far less than the energy of the information bits, the signs of Z_{2k} and Z_{2k+1} are determined by the signs of the data bits b_{2k} and b_{2k+1}, respectively. Thus, regardless of the influences of the noise, the data bits can be demodulated according to the rule as follows:

$$b_n = \begin{cases} 1, & \text{for } Z_j > 0 \\ -1, & \text{for } Z_j < 0. \end{cases}$$

B. Performance Evaluation

In this section, we evaluate the ability of the proposed DCSK in resisting transmission noise when using different chaotic maps as the chaotic generator. To provide a clear comparison, all the control parameters for the competing 3-D chaotic maps are set as the same settings as them in Section V. Because the addition white Gaussian noise (AWGN) is one of the most common occurrence noises in different transmission channels, we test the BERs of the proposed DCSK in the AWGN channel against various levels of noise and various spread factors M.

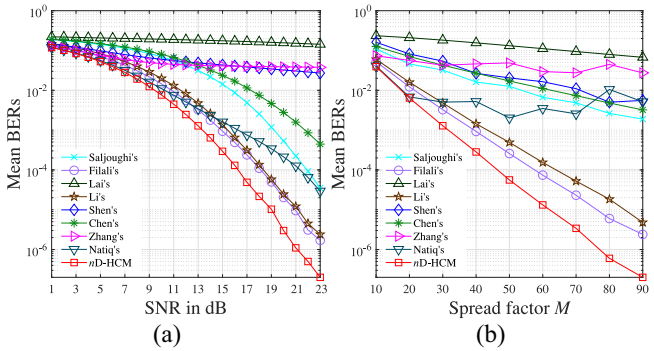

Fig. 10. BERs of the proposed DCSK using different 3-D chaotic maps when (a) transmission noise levels $SNR \in \{1, 2, \ldots, 23\}$ with spread factor $M = 30$, and (b) spread factors $M \in \{10, 20, \ldots, 90\}$ with transmission noise level $SNR = 13$ dB.

Two sets of experiments are designed to evaluate the BERs of the proposed DCSK using various 3-D chaotic maps as the chaotic generator. The first set measures the BERs under various noise levels when setting the spread factor $M = 30$. For all the chaotic maps, we first randomly generate a 100 000-length bit binary as the transmitted data, and then generate a chaotic sequence with a randomly selected parameter setting, and finally calculate the BERs between the recovered bits and the original data bits under different signal-to-noise-ratios (SNRs) SNR $\in \{1, 2, \ldots, 23\}$. To provide a stable result, 100 experiments are performed and the mean BERs are calculated and plotted in Fig. 10(a). The results display that when using the chaotic maps produced by our generation method, the proposed DCSK obtains smaller BERs than using other chaotic maps under various levels of AWGN.

The second set of experiments tests the BERs under different spread factors M when fixing the noise level as SNR = 13 dB. The experiments for each chaotic map are set the same as in the first set of experiments and the mean BERs of 100 experiments are calculated against spread factors $M \in \{10, 20, \ldots, 90\}$. Fig. 10(b) depicts the mean BERs of the proposed DCSK applying various chaotic maps as the chaotic generator. As can be seen, with different spread factors, the DCSK using the chaotic maps generated by our method also obtain much smaller BERs than using other chaotic maps. These indicate that when being applied to secure communication, the chaotic maps produced by our method can show good performance in resisting transmission noise, and thus are suitable for this application.

VII. Conclusion

In this article, we proposed an n-dimensional hyperchaotic map (nD-HCM) generation method that can generate HD chaotic maps with expected dynamics and robust hyperchaotic behaviors. First, a general form of the proposed nD-HCM is constructed using n parametric polynomials. Then, the entity and coefficient parameter matrices of the proposed nD-HCM are configured according to the Gershgorin-type theorem. Theoretical analysis indicates that the constructed nD-HCM has n positive LEs and thus can achieve robust hyperchaotic behaviors. Two examples are generated and their properties

$$
\begin{aligned}
Z_{2k} &= \sum_{i=(2k+1)M+1}^{2(k+1)M} (s_{i-M}+\xi_{i-M})(s_i+\xi_i) \\
&= \frac{\sqrt{2}}{2} \sum_{i=(2k+1)M+1}^{(2k+3/2)M} (x_{i-M}+\xi_{i-M})\left(b_{2k}x_{i-M}+b_{2k+1}x_{2(i-kM-M)-1}+\xi_i\right) \\
&\quad + \frac{\sqrt{2}}{2} \sum_{i=(2k+3/2)M+1}^{2(k+1)M} (x_{i-M}+\xi_{i-M})\left(b_{2k}x_{i-M}+b_{2k+1}x_{2(i-kM-3/2M)}+\xi_i\right) \\
&= \frac{\sqrt{2}}{2} \sum_{i=(2k+1)M+1}^{2(k+1)M} b_{2k}x_{i-M}^2 + \frac{\sqrt{2}}{2} \sum_{i=(2k+1)M+1}^{2(k+1)M} (b_{2k}x_{i-M}\xi_{i-M}+x_{i-M}\xi_i+\xi_i\xi_{i-M}) \\
&\quad + \frac{\sqrt{2}}{2} \sum_{i=(2k+1)M+1}^{(2k+3/2)M} b_{2k+1}x_{2(i-kM-M)-1}(x_{i-M}+\xi_{i-M}) + \frac{\sqrt{2}}{2} \sum_{i=(2k+3/2)M+1}^{2(k+1)M} b_{2k+1}x_{2(i-kM-3/2M)}(x_{i-M}+\xi_{i-M}). \qquad (34)
\end{aligned}
$$

$$
\begin{aligned}
Z_{2k+1} &= \sum_{i=(2k+1)M+1}^{2(k+1)M} \left(s_{i-M}^*+\xi_{i-M}^*\right)(s_i+\xi_i) \\
&= \frac{\sqrt{2}}{2} \sum_{i=(2k+1)M+1}^{(2k+3/2)M} \left(x_{2(i-kM-M)-1}+\xi_{2(i-kM-M)-1}\right)\left(b_{2k}x_{i-M}+b_{2k+1}x_{2(i-kM-M)-1}+\xi_i\right) \\
&\quad + \frac{\sqrt{2}}{2} \sum_{i=(2k+3/2)M+1}^{2(k+1)M} \left(x_{2(i-kM-3/2M)}+\xi_{2(i-kM-3/2M)}\right)\left(b_{2k}x_{i-M}+b_{2k+1}x_{2(i-kM-3/2M)}+\xi_i\right) \\
&= \frac{\sqrt{2}}{2} \sum_{i=(2k+1)M+1}^{2(k+1)M} b_{2k+1}x_{i-M}^2 + \frac{\sqrt{2}}{2} \sum_{i=(2k+1)M+1}^{2(k+1)M} b_{2k+1}x_{i-M}\xi_{i-M} \\
&\quad + \frac{\sqrt{2}}{2} \sum_{i=(2k+1)M+1}^{(2k+3/2)M} \left(b_{2k}x_{2(i-kM-M)-1}x_{i-M}+x_{2(i-kM-M)-1}\xi_i+b_{2k}\xi_{2(i-kM-M)-1}x_{i-M}+\xi_{2(i-kM-M)-1}\xi_i\right) \\
&\quad + \frac{\sqrt{2}}{2} \sum_{i=(2k+3/2)M+1}^{2(k+1)M} \left(b_{2k}x_{2(i-kM-3/2M)}x_{i-M}+x_{2(i-kM-3/2M)}\xi_i+b_{2k}\xi_{2(i-kM-3/2M)}x_{i-M}+\xi_{2(i-kM-3/2M)}\xi_i\right). \qquad (35)
\end{aligned}
$$

are analyzed to manifest the effectiveness of the proposed method. Performance evaluations display that the HD chaotic maps generated by the proposed method can obtain better performance than many representative HD chaotic maps. To exhibit the practical application of the proposed nD-HCMs, we applied them to the secure communication. Experimental results show that the secure communication scheme using the nD-HCMs generated by our method has significantly better performance than it using other chaotic maps. Since the newly constructed HCMs have high-performance indicators, they can be applied to many chaos-based engineering applications. Our future work will study the application of these maps in image security application.

APPENDIX

The detailed descriptions of (32) and (33) are as shown in (34) and (35), as shown at the top of the page, respectively.

REFERENCES

[1] Y. Wang, W. X. Zheng, and H. Zhang, "Dynamic event-based control of nonlinear stochastic systems," *IEEE Trans. Autom. Control*, vol. 62, no. 12, pp. 6544–6551, Dec. 2017.

[2] S. Dong, Z.-G. Wu, P. Shi, H. Su, and T. Huang, "Quantized control of Markov jump nonlinear systems based on fuzzy hidden Markov model," *IEEE Trans. Cybern.*, vol. 49, no. 7, pp. 2420–2430, Jul. 2019.

[3] H. Lin et al., "An extremely simple multiwing chaotic system: Dynamics analysis, encryption application, and hardware implementation," *IEEE Trans. Ind. Electron.*, vol. 68, no. 12, pp. 12708–12719, Dec. 2021.

[4] C. Peng, J. Zhang, and Q.-L. Han, "Consensus of multiagent systems with nonlinear dynamics using an integrated sampled-data-based event-triggered communication scheme," *IEEE Trans. Syst., Man, Cybern., Syst.*, vol. 49, no. 3, pp. 589–599, Mar. 2019.

[5] N. Lin, X. Chen, H. Lu, and X. Li, "Chaotic weights: A novel approach to protect intellectual property of deep neural networks," *IEEE Trans. Comput-Aided Design Integ. Circuits Syst.*, vol. 40, no. 7, pp. 1327–1339, Jul. 2021.

[6] M. Hirsch, S. Smale, and R. Devaney, *Differential Equations, Dynamical Systems, and an Introduction to Chaos*. Oxford, U.K.: Academic, 2012.

[7] X. Chen, J. Cao, J. H. Park, and J. Qiu, "Finite-time control of multiple different-order chaotic systems with two network synchronization modes," *Circuits, Syst., Signal Process.*, vol. 37, no. 3, pp. 1081–1097, 2018.

[8] K.-L. Du and M. N. S. Swamy, "Hopfield networks, simulated annealing, and chaotic neural networks," in *Neural Networks and Statistical Learning*. London, U.K.: Springer, 2019, pp. 173–200.

[9] H. G. Schuster and W. Just, *Deterministic Chaos: An Introduction*. Weinheim, Germany: Wiley, 2006.

[10] B. Kaviarasan, O.-M. Kwon, M. J. Park, and R. Sakthivel, "Integrated synchronization and anti-disturbance control design for fuzzy model-based multiweighted complex network," *IEEE Trans. Syst., Man, Cybern., Syst.*, vol. 51, no. 10, pp. 6330–6341, Oct. 2021.

[11] S. Chen, S. Yu, J. Lü, G. Chen, and J. He, "Design and FPGA-based realization of a chaotic secure video communication system," *IEEE Trans. Circuits Syst. Video Technol.*, vol. 28, no. 9, pp. 2359–2371, Sep. 2018.

[12] S. Gao, Y. Yu, Y. Wang, J. Wang, J. Cheng, and M. Zhou, "Chaotic local search-based differential evolution algorithms for optimization," *IEEE Trans. Syst., Man, Cybern., Syst.*, vol. 51, no. 6, pp. 3954–3967, Jun. 2021.
[13] L. Chen, C. Li, and C. Li, "Security measurement of a medical image communication scheme based on chaos and DNA," *J. Vis. Commun. Image Represent.*, vol. 83, Feb. 2022, Art. no. 103424.
[14] S. Liu, C. Li, and Q. Hu, "Cryptanalyzing two image encryption algorithms based on a first-order time-delay system," *IEEE MultiMedia*, vol. 29, no. 1, pp. 74–84, Jan.–Mar. 2022.
[15] J. C. L. Chan, T. H. Lee, and C. P. Tan, "Secure communication through a chaotic system and a sliding-mode observer," *IEEE Trans. Syst., Man, Cybern., Syst.*, vol. 52, no. 3, pp. 1869–1881, Mar. 2022.
[16] Y. Zhao, W. Zhang, H. Su, and J. Yang, "Observer-based Synchronization of chaotic systems satisfying incremental quadratic constraints and its application in secure communication," *IEEE Trans. Syst., Man, Cybern., Syst.*, vol. 50, no. 12, pp. 5221–5232, Dec. 2020.
[17] N. Wang, C. Li, H. Bao, M. Chen, and B. Bao, "Generating multi-scroll Chua's attractors via simplified piecewise-linear Chua's diode," *IEEE Trans. Circuits Syst. I, Reg. Papers*, vol. 66, no. 12, pp. 4767–4779, Dec. 2019.
[18] Z. Hua and Y. Zhou, "Exponential chaotic model for generating robust chaos," *IEEE Trans. Syst., Man, Cybern., Syst.*, vol. 51, no. 6, pp. 3713–3724, Jun. 2021.
[19] C. Li, D. Lin, J. Lü, and F. Hao, "Cryptanalyzing an image encryption algorithm based on autoblocking and electrocardiography," *IEEE MultiMedia*, vol. 25, no. 4, pp. 46–56, Dec. 2018.
[20] L. Liu, J. Lin, S. Miao, and B. Liu, "A double perturbation method for reducing dynamical degradation of the digital baker map," *Int. J. Bifurc. Chaos*, vol. 27, no. 7, 2017, Art. no. 1750103.
[21] Y. Deng and Y. Li, "A 2D Hyperchaotic discrete Memristive map and application in reservoir computing," *IEEE Trans. Circuits Syst. II, Exp. Briefs*, vol. 69, no. 3, pp. 1817–1821, Mar. 2022.
[22] Y. Li, C. Li, S. Zhang, G. Chen, and Z. Zeng, "A self-reproduction hyperchaotic map with compound lattice dynamics," *IEEE Trans. Ind. Electron.*, vol. 69, no. 10, pp. 10564–10572, Oct. 2022.
[23] L. Lin, M. Shen, H. C. So, and C. Chang, "Convergence analysis for initial condition estimation in coupled map lattice systems," *IEEE Trans. Signal Process.*, vol. 60, no. 8, pp. 4426–4432, Aug. 2012.
[24] S. Feng, M. Han, J. Zhang, T. Qiu, and W. Ren, "Learning both dynamic-shared and dynamic-specific patterns for chaotic time-series prediction," *IEEE Trans. Cybern.*, vol. 52, no. 6, pp. 4115–4125, Jun. 2022.
[25] S. Ergün, "On the security of chaos based 'true' random number generators," *IEICE Trans. Fundam. Electron., Commun. Comput. Sci.*, vol. 99, no. 1, pp. 363–369, 2016.
[26] S. Wiggins, *Introduction to Applied Nonlinear Dynamical Systems and Chaos*, vol. 2. New York, NY, USA: Springer, 2003.
[27] A. Shokouh Saljoughi and H. Mirvaziri, "A new method for image encryption by 3D chaotic map," *Pattern Anal. Appl.*, vol. 22, no. 1, pp. 243–257, 2018.
[28] R. L. Filali, M. Benrejeb, and P. Borne, "On observer-based secure communication design using discrete-time hyperchaotic systems," *Commun. Nonlinear Sci. Numer. Simulat.*, vol. 19, no. 5, pp. 1424–1432, 2014.
[29] Q. Lai, P. D. K. Kuate, F. Liu, and H. H.-C. Iu, "An extremely simple chaotic system with infinitely many coexisting attractors," *IEEE Trans. Circuits Syst. II, Exp. Briefs*, vol. 67, no. 6, pp. 1129–1133, Jun. 2020.
[30] A. Lassoued and O. Boubaker, "On new chaotic and hyperchaotic systems: A literature survey," *Nonlinear Anal.-Model Control*, vol. 21, no. 6, pp. 770–789, 2016.
[31] C. Shen, S. Yu, J. Lü, and G. Chen, "Constructing hyperchaotic systems at will," *Int. J. Circuit Theory Appl.*, vol. 43, no. 12, pp. 2039–2056, 2015.
[32] Q. Wu, F. Zhang, Q. Hong, X. Wang, and Z. Zeng, "Research on cascading high-dimensional isomorphic chaotic maps," *Cogn. Neurodyn.*, vol. 15, pp. 157–167, Mar. 2020.
[33] C. Shen, S. Yu, J. Lü, and G. Chen, "Designing hyperchaotic systems with any desired number of positive Lyapunov exponents via a simple model," *IEEE Trans. Circuits Syst. I, Reg. Papers*, vol. 61, no. 8, pp. 2380–2389, Aug. 2014.
[34] Y. Wu, Z. Hua, and Y. Zhou, "*N*-dimensional discrete cat map generation using laplace expansions," *IEEE Trans. Cybern.*, vol. 46, no. 11, pp. 2622–2633, Nov. 2018.
[35] L. Qi, "Some simple estimates for singular values of a matrix," *Linear Algebra Appl.*, vol. 56, pp. 105–119, Jan. 1984.
[36] J. He, Y. M. Liu, J. K. Tian, and Z. R. Ren, "New inclusion sets for singular values," *J. Inequal. Appl.*, vol. 2017, p. 8, 2017.
[37] U. Schwengelbeck and F. Faisal, "Definition of Lyapunov exponents and KS entropy in quantum dynamics," *Phys. Lett. A*, vol. 199, nos. 5–6, pp. 281–286, 1995.
[38] L. Lu and C. E. M. Pearce, "Some new bounds for singular values and eigenvalues of matrix products," *Ann. Oper. Res.*, vol. 98, no. 1, pp. 141–148, 2000.
[39] L. Dieci, R. D. Russell, and E. S. Van Vleck, "On the Compuation of Lyapunov exponents for continuous dynamical systems," *SIAM J. Numer. Anal.*, vol. 34, no. 1, pp. 402–423, 1997.
[40] C. Li, B. Feng, S. Li, J. Kurths, and G. Chen, "Dynamic analysis of digital chaotic maps via state-mapping networks," *IEEE Trans. Circuits Syst. I, Reg. Papers*, vol. 66, no. 6, pp. 2322–2335, Jun. 2019.
[41] C. Li, K. Tan, B. Feng, and J. Lü, "The graph structure of the generalized discrete Arnold's cat map," *IEEE Trans. Comput.*, vol. 71, no. 2, pp. 364–377, Feb. 2022.
[42] L. Lacasa and J. Gómez-Gardenes, "Correlation dimension of complex networks," *Phys. Rev. Lett.*, vol. 110, no. 16, 2013, Art. no. 168703.
[43] Z. Spiclin, B. Likar, and F. Pernus, "Groupwise registration of multimodal images by an efficient joint entropy minimization scheme," *IEEE Trans. Image Process.*, vol. 21, pp. 2546–2558, 2012.
[44] Y. Zhang, H. Xiang, S. Zhang, and L. Liu, "Construction of high-dimensional cyclic symmetric chaotic map with one-dimensional chaotic map and its security application," *Multimed. Tools Appl.*, vol. 82, pp. 17715–17740, May 2023.
[45] H. Natiq, S. Banerjee, S. He, M. R. M. Said, and A. Kilicman, "Designing an M-dimensional nonlinear model for producing hyperchaos," *Chaos Solitons Fractals*, vol. 114, pp. 506–515, Sep. 2018.
[46] W. Li, W. Yan, R. Zhang, C. Wang, and Q. Ding, "A new 3D discrete Hyperchaotic system and its application in secure transmission," *Int. J. Bifurc. Chaos*, vol. 29, no. 14, 2019, Art. no. 1950206.
[47] Z. Lin, S. Yu, J. Lu, S. Cai, and G. Chen, "Design and ARM-embedded implementation of a chaotic map-based real-time secure video communication system," *IEEE Trans. Circuits Syst. Video Technol.*, vol. 25, no. 7, pp. 1203–1216, Jul. 2015.

Yinxing Zhang received the M.S. degree in fundamental mathematics from the Guilin University of Electronic Technology, Guilin, China, in 2019. He is currently pursuing the Ph.D. degree in computer science and technology with the School of Computer Science and Technology, Harbin Institute of Technology, Shenzhen, Shenzhen, China.

His current research interests include chaotic system and nonlinear system control.

Zhongyun Hua (Senior Member, IEEE) received the B.S. degree in software engineering from Chongqing University, Chongqing, China, in 2011, and the M.S. and Ph.D. degrees in software engineering from the University of Macau, Macau, China, in 2013 and 2016, respectively.

He is currently an Associate Professor with the School of Computer Science and Technology, Harbin Institute of Technology, Shenzhen, Shenzhen, China. His works have appeared in prestigious venues, such as IEEE TRANSACTIONS ON DEPENDABLE AND SECURE COMPUTING, IEEE TRANSACTIONS ON SIGNAL PROCESSING, IEEE TRANSACTIONS ON IMAGE PROCESSING, IEEE TRANSACTIONS ON CYBERNETICS, IEEE TRANSACTIONS ON SYSTEMS, MAN, AND CYBERNETICS: SYSTEMS, and *ACM Multimedia*. He has published more than 70 papers on the subject, receiving more than 5000 citations. His current research interests are focused on chaotic system, multimedia security, and secure cloud computing.

Dr. Hua has been recognized as a Highly Cited Researcher 2022. He is currently an Associate Editor of *International Journal of Bifurcation and Chaos*.

Han Bao (Member, IEEE) received the B.S. degree in landscape design from the Jiangxi University of Finance and Economics, Nanchang, China, in 2015, the M.S. degree in art and design from Changzhou University, Changzhou, China, in 2018, and the Ph.D. degree in nonlinear system analysis and measurement technology from the Nanjing University of Aeronautics and Astronautics, Nanjing, China, in 2021.

In 2019, he visited the Computer Science Department, The University of Auckland, Auckland, New Zealand. He is currently a Lecturer with the School of Microelectronics and Control Engineering, Changzhou University. His research interests include memristive neuromorphic circuit, nonlinear circuits and systems, and artificial intelligence.

Hejiao Huang received the B.S. and M.S. degrees in mathematics from Shaanxi Normal University, Xi'an, China, in 1996 and 1999, respectively, and the Ph.D. degree in computer science from the City University of Hong Kong, Hong Kong, in 2004.

She was an Invited Professor with INRIA, Bordeaux, France. She is currently a Professor with the Harbin Institute of Technology, Shenzhen, Shenzhen, China. Her research interests include cloud computing, network security, trustworthy computing, and formal methods for system design and wireless networks.

Yicong Zhou (Senior Member, IEEE) received the B.S. degree in electrical engineering from Hunan University, Changsha, China, in 1992, and the M.S. and Ph.D. degrees in electrical engineering from Tufts University, Medford, MA, USA, in 2008 and 2010, respectively.

He is a Professor with the Department of Computer and Information Science, University of Macau, Macau, China. His research interests include image processing, computer vision, machine learning, and multimedia security.

Dr. Zhou was recognized as one of the World's Top 2% Scientists and one of the Highly Cited Researchers in 2020 and 2021. He received the Third Price of Macao Natural Science Award as a sole winner in 2020 and was a co-recipient in 2014. He has been a Leading Co-Chair of the Technical Committee on Cognitive Computing of the IEEE Systems, Man, and Cybernetics Society since 2015. He serves as an Associate Editor for IEEE TRANSACTIONS ON NEURAL NETWORKS AND LEARNING SYSTEMS, IEEE TRANSACTIONS ON CIRCUITS AND SYSTEMS FOR VIDEO TECHNOLOGY, and IEEE TRANSACTIONS ON GEOSCIENCE AND REMOTE SENSING. He is a Fellow of the Society of Photo-Optical Instrumentation Engineers.